Uncovering Chemical Homology of Superheavy Elements: A Close Look at Astatine

Yuriy A. Demidov,[†] Alexander A. Shalaevsky,[‡] Alexander V. Oleynichenko,[†] and Alexander A. Rusakov[*,¶]

†*B. P. Konstantinov Petersburg Nuclear Physics Institute of National Research Center "Kurchatov Institute" (NRC "Kurchatov Institute" – PNPI), Orlova Roscha, 1, 188300 Gatchina, Russia*

‡*St. Petersburg Electrotechnical University "LETI", 197376 St. Petersburg, Russia*

¶*Department of Chemistry, Oakland University, Rochester, Michigan, 48309 USA*

E-mail: rusakov@oakland.edu

Abstract

The fascination with superheavy elements (SHE) spans the nuclear physics, astrophysics, and theoretical chemistry communities. Extreme relativistic effects govern these elements' chemistry and challenge the traditional notion of the periodic law. The experimental quest for SHE critically depends on theoretical predictions of these elements' properties, especially chemical homology, which allows for successful prototypical experiments with more readily available lighter homologues of SHE. This work is a comprehensive quantum-chemical investigation into astatine (At) as a non-intuitive homologue of element 113, nihonium (Nh). Combining relativistic coupled-cluster and density functional theory approaches, we model the behaviour of At and AtOH in thermochromatographic experiments on a pristine gold surface. Insights into the electronic structure of AtOH and NhOH and accurate estimates of At–gold and AtOH–gold adsorption energies rationalize recent experimental findings and justify the use of At as a chemical homologue of Nh for the successful design of future experiments on Nh detection and chemical characterization.

I Introduction

Long-lived isotopes of superheavy elements (SHEs) discovered in ^{48}Ca nuclear fusion reactions with actinide targets suggest that the island of particularly shell-stabilised nuclei[1] could be within reach. Recently, attention to superheavy elements (SHE) has extended to astrophysics: new studies suggest that SHE can be observed in kilonovae, rendering these elements more than short-lived peculiarities of artificial nucleosynthesis.[2,3] While the emergence of new elements is already a fantastic discovery, the longevity of certain isotopes inspires experimental and theoretical investigations into these elements' chemistry, advancing the quest for SHE[4,5] as the ultimate test of the periodic law.[6–10] Such investigations resulted in successful chemical identification of copernicium (element 112, Cn),[11] flerovium (element 114, Fl),[12,13] and nihonium (element 113, Nh),[14] as confirmed at the fourth IUPAC/IUPAP Joint Working Party.[15]

Gas thermochromatography on a gold surface[16] is a unique SHEs' chemical detection method. However, these highly sophisticated and expensive experiments yield only limited information on the chemical properties of SHEs. Furthermore, the correct and detailed interpretation of the available experimental data is only possible with preliminary theoretical modelling. Therefore, the quantitative theoretical prediction of the SHEs' interactions with a gold surface is integral to identifying these elements.

Strong relativistic effects suggest dramatic dissimilarities in the chemical behaviour of SHEs and their formal lighter homologues.[17,18] Experiments show that for atomic copernicium (Cn, Z=112) and flerovium (Fl, Z=114), the temperatures and adsorption enthalpies on a gold surface, $\Delta H_{\mathrm{ads}}^{\mathrm{Au}}$ are close to each other, $-\Delta H_{\mathrm{ads}}^{\mathrm{Au}}(\mathrm{Cn}) = 52^{+4}_{-3}$ kJ/mol and $-\Delta H_{\mathrm{ads}}^{\mathrm{Au}}(\mathrm{Fl}) = 34^{+54}_{-11}$ kJ/mol. For their respective immediate homologues — mercury and lead — these values are $-\Delta H_{\mathrm{ads}}^{\mathrm{Au}}(\mathrm{Hg}) = 98 \pm 3$ kJ/mol[19] and $-\Delta H_{\mathrm{ads}}^{\mathrm{Au}}(\mathrm{Pb}) = 295$ kJ/mol.[13] Thus, Fl displays the properties fairly close to quasi-inert closed-shell Hg and Cn and is drastically dissimilar to its formal homologue Pb. This is the direct consequence of the strong $7p_{1/2}$–$7p_{3/2}$ spin-orbit splitting and the relativistic stabilisation of the $7p_{1/2}$ shell. The realisation of an almost pure j-j coupling scheme[20] gives rise

to a closed-shell $6d^{10}7s^27p_{1/2}^2$ lowest-energy configuration of the Fl atom, resulting in the same $^1S_0$ ground state as in Hg ($5d^{10}6s^2$) and Cn ($6d^{10}7s^2$). Despite manifest deviations in the chemical properties of SHEs from the trends observed in their lighter formal homologues in the respective groups of the periodic table, finding chemical homologues is a practically meaningful issue,[21–23] especially in light of the ongoing experimental studies of nihonium (Nh, Z=113).[24]

The theoretically predicted adsorption enthalpy of single Nh atoms on a gold surface ($-\Delta H_{\rm ads}^{\rm Au}({\rm Nh}) = 106 \pm 10$ kJ/mol[25]) differs substantially from the experimentally measured value for its formal homologue, thallium ($-\Delta H_{\rm ads}^{\rm Au}({\rm Tl}) = 270 \pm 10$ kJ/mol[26]). Even though both Tl($5d^{10}6s^26p_{1/2}^1$) and Nh($6d^{10}7s^27p_{1/2}^1$) are open-shell atoms with the $^2P_{1/2}$ ground state, the Tl–Nh chemical homology appears tenuous for calibrating the experiments on Nh.

However, the placement of Nh between two quasi-inert closed-shell Cn and Fl — a unique feature of the 7$^{\rm th}$ row of the periodic table — allows for an interpretation of the electronic structure of a Nh atom as a hole in the closed 7p subshell of a Fl atom.[27,28] Given the substantial dissimilarities between Nh and Tl, the next closest realisation of a single p-shell hole is in astatine, whose $^2P_{3/2}$ ground state is dominated by the At($5d^{10}6s^26p_{1/2}^26p_{3/2}^3$) configuration. Even despite different angular distribution functions of $7p_{1/2}$ and $6p_{3/2}$ spinors,[29–31] similarities in the chemical behaviour of Nh and At transpire in a comparative study of their hydroxide molecules, whose formation is possible in the presence of oxygen and water.[32] Demidov and Zaitsevskii[33] estimated the energy of the hydroxyl group elimination at 0 K at *ca.* 188 kJ/mol for NhOH, and the respective values for TlOH and AtOH at 319 and 174 kJ/mol. These estimates reveal that the chemical properties of Nh are closer to those of At than the formal homologue Tl and suggest At as a pseudo-homologue of Nh[34] and a plausible lighter candidate to optimise the experimental conditions for further Nh chemistry explorations.

Several theoretical estimates of elemental At adsorption energy on the (111) gold surface with relativistic density functional theory (DFT) are available: 130 ± 10 kJ/mol using finite Au clusters,[35] and 175 kJ/mol,[36‡] 184 kJ/mol,[38] and 189 kJ/mol[39] from periodic calculations. The

[0]‡ Tanudji *et al.*[36] give 138 kJ/mol with respect to At_2 in the dissociation limit. We normalise it to atomic At using $D_e(At_2)$=75.0 kJ/mol.[37]

result derived from thermochromatographic data is 147 ± 15 kJ/mol.[40] Ryzhkov *et al.*[38] ascribe the discrepancy between their results and those in ref. 35, albeit without supporting numerical data and despite a better agreement between ref. 35 and experiment,[40] to "obvious limitations" of the cluster model, the neglect of cluster relaxation caused by adsorption, and the use of the DFT model without a dispersion correction. However, Tanudji *et al.*[36] evaluate the dispersion contribution to the At – Au (111) adsorption energy at *ca.* 50 kJ/mol, which is 28% of their total value.

Astatine or nihonium species other than single atoms possibly present in gas thermochromatography experiments further complicate the detection of these elements based on measuring the adsorption energy on a gold surface.[32,40] The quantities of astatine species are insufficient for standard spectroscopic techniques to determine their molecular structure. Thus, any interpretation of the experimental outcome hinges on testing the hypotheses on the astatine molecular species in the carrier gas using quantitative predictions of these species' interactions with gold. The available thermochromatographic data do not appear to have decisively settled the debate on the particular AtO_xH_y molecules observed.[32,40] In the most recent online gas thermochromatography experiments, Chiera *et al.*[32] detect a volatile At species with the adsorption energy on a gold surface ≥ 90 kJ/mol and argue in favour of AtOH as the most plausible candidate.

Compared to the case of elemental At, an even more significant discrepancy in theoretical estimates of AtOH – Au (111) adsorption energy exists: 90 ± 10[35] *vs.* 189[38] kJ/mol. The latter estimate is remarkably close to the same authors' At – Au (111) adsorption energy, and they attribute its significant difference from the ref. 35 one to the same factors as for elemental At, also without any numerical details. The estimate in ref. 35 appears in much better agreement with the experimental data, especially ref. 32. However, exploring the role of dispersion interactions in AtOH binding with gold remains worthwhile.

This paper presents a comprehensive quantum-chemical investigation into astatine's potential chemical homology with superheavy elements. Specifically, we address the chemical reactivity of AtOH in comparison to TlOH and NhOH, assess computational methodology for modelling At — Au(111) interactions, and revisit the discrepancies in theoretical estimates of At and AtOH

adsorption energies on a gold surface. Finally, we suggest a plausible explanation of AtOH formation and stability on Au(111).

II Computational details

A Relativistic effective core potentials

Scalar and spin-dependent relativistic effects are critically important in modelling the electronic structure of astatine compounds.[41] In all our DFT and *ab initio* wavefunction calculations involving Au, Tl, At, or Nh atoms, we incorporate these effects using semi-local versions of highly accurate[42,43] shape-consistent generalised relativistic effective core potentials (RECPs) by Mosyagin *et al.*[44–46] These RECPs replace 60 core electrons of Au, Tl, and At, and 90 of Nh. The RECPs for Tl and At also include the lowest-order quantum electrodynamics contributions.[47] By employing the RECP Hamiltonian, we economically account for the relativistic effects within the two-component (2c) formalism without compromising the calculations' accuracy. We treat all electrons for O and H atoms explicitly. Because of the insignificance of relativistic effects in O and H, we use the non-relativistic Coulomb Hamiltonian in the calculations of individual O and OH species.

B Relativistic coupled-cluster calculations of X-OH (X = Tl, At, Nh) first excitation and binding energies

The magnitude of the energy gap between the ground and the first excited electronic state, or the electron promotion energy, which for stable closed-shell systems is usually referred to as the singlet-triplet gap, tends to negatively correlate with chemical reactivity, thus providing its rough measure.[48] In molecules with atoms as heavy as Tl, At, and especially Nh, spin-states are not well-defined because of strong spin-dependent relativistic effects ("spin-orbit coupling"). Therefore, the gap between the relativistic ground and the first excited states is the closest analogy of the singlet-

triplet gap. Such excited states originate from promoting an electron from the highest occupied molecular spinor to the lowest virtual Kramers pair.

The relativistic Fock-space coupled-cluster method with single and double excitations (FS RCCSD)[49–51] is an economical alternative to equation-of-motion CCSD yet rigorous approach to calculating vertical excitation energies to the lowest-lying electronic states. Its typical uncertainty is *ca.* 0.1 eV or lower (see review 51 and references therein). We calculate target singly-excited ("triplet") states in the one hole and one particle ($1h1p$) Fock space sector[52,53] with respect to the closed-shell ground state considered as the Fermi vacuum. Model spaces comprise the determinants obtained by single excitations of electrons occupying 4 (TlOH), 5 (AtOH) and 7 (NhOH) Kramers pairs of the highest occupied molecular spinors (HOMS) to 15 (TlOH), 11 (AtOH) and 14 (NhOH) Kramers pairs of the lowest unoccupied molecular spinors (LUMS).

The apparent variability of the chosen active spaces reflects noticeable, albeit unsurprising, differences in the spinors' energy spectra, even for presumed chemical homologues. Assuming a reasonable core–valence separation to be of a few eV, we choose active holes counting from the HOMS down until we encounter such a gap. We find these gaps to be 6.1 eV between HOMS−3 and HOMS−4 in TlOH, 8.3 eV between HOMS−4 and HOMS−5 in AtOH, and 3.2 eV between HOMS−6 and HOMS−7 in NhOH. As expected, the energy spacing is much smaller across low-lying unoccupied spinors. We require the energy gap between active and virtual particles to exceed 0.5 eV. This criterion results in the following active–virtual particles separations: 0.8 eV between LUMS+14 and LUMS+15 in TlOH, 0.7 eV between LUMS+10 and LUMS+11 in AtOH, and 0.9 eV between LUMS+13 and LUMS+14 in NhOH. Our *a posteriori* analysis indicates that this choice generates active spaces substantially larger than is necessary to include the determinants that dominate in the first excited states, thus ensuring convergence with respect to the active-space size. We enclose sample output files of these calculations in ESI.

To bypass the intruder-state problem, we use the intermediate Hamiltonian formulation of FS RCCSD for incomplete main model spaces recently proposed by Zaitsevskii *et al.*[47] and implemented in the EXP-T program.[54,55] This FS RCCSD code relies on one-electron spinors

and transformed molecular integrals from the DIRAC19 program package.[56,57] We use quadruple-zeta quality basis sets for Tl, At, and Nh from refs. 58,59 adapted for the chosen RECP model,[60] and aug-cc-pVQZ-DK[61] basis sets for H and O.

To calculate hydroxyl group elimination energies D_0, we apply the single-reference relativistic 2c-CCSD(T) method[62] as implemented in the DIRAC19 program[56,57] and the same basis sets as in FS RCCSD calculations. We also apply counterpoise correction to compensate for the basis-set superposition error and include zero-point energy (ZPE) from harmonic vibrational frequencies calculated at the DFT/B88P86 level by Demidov and Zaitsevskii.[33] The analysis of these results in Sec. A also serves as an additional assessment of the DFT approaches' quality.

C Relativistic density functional theory calculation of adsorption properties

With relativistic coupled-cluster methods becoming prohibitively demanding for polyatomic molecules or clusters, we resort to two-component relativistic density functional theory (2c-RDFT) to simulate the adsorption of At, AtOH, O, and OH on a gold surface. In 2c-RDFT calculations, we employ the collinear version of the method in NWCHEM[63] for preliminary geometry-optimisation calculations. However, we derive the ultimate results reported in this work from the more rigorous non-collinear approach implemented in TURBOMOLE[64,65] and (identically) in an older TURBOMOLE-based stand-alone programme.[66] In these calculations, we use the two-electron integrals cutoff $1.0 \cdot 10^{-16}$ and the finest DFT quadrature grid (\$grid 7). We apply the convergence criterion of $1.0 \cdot 10^{-7}$ a.u. to energies and $1.0 \cdot 10^{-4}$ a.u. to gradients.

Choosing an appropriate XCF approximation for relativistic electronic-structure calculations of heavy-element species is a lingering problem[67] that persists in the case of At compounds.[68] In the absence of relativistic XCFs suitable for molecular quantum-chemical modelling,[69] we base our choice on previously documented successes and additional reliability tests in the present work.

Based on the first ionisation potential (IP) and electron affinity (EA) of At, EA of O, the OH group elimination energy from AtOH, and the bond dissociation energies (D_e) of AtO, AtO^+, and AtAu, a practically non-empirical hybrid XCF PBE0[74,75] is a well-justified choice overall.

Table 1: Calculated and experimental values for the first ionisation potential and the electron affinity of astatine, the electron affinity of oxygen, and bond dissociation energies of astatine compounds. In all DFT calculations, we use the largest DFT-specific basis sets for At (PSO-Lc+g) and Au (RDFT+g, see main text below) and the aug-pcseg-2 sets for H and O. All energy values are in kJ/mol.

	B88P86	PBE0	LRC-ωPBEh	Theor.	Exptl.
At, IP	897	886	884	898[70]	899[70]
At, EA	230	221	214	233[71]	233[71]
O, EA	181	136	143	141[72]	141[73]
AtOH, D_e [a]	203	174	173	180[33]	–
AtO^+, D_e [b]	273	186	185	224[37]	–
AtO, D_e	260	193	187	201[c]	–
AtAu, D_e	192	182	163	186[37]	–

[a] The dissociation energy here is $D_e = E(\mathrm{At}) + E(\mathrm{OH}) - E(\mathrm{AtOH})$.
[b] The dissociation energy here is $D_e = E(\mathrm{At}^+) + E(\mathrm{O}) - E(\mathrm{AtO}^+)$.
[c] The 2c-CCSD(T)/CBS value in present work is calculated as in ref. 37.

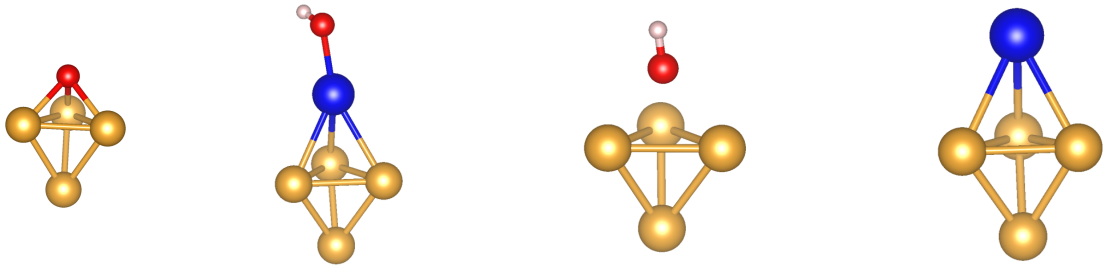

Figure 1. Small X–Au_4 (M = O, AtOH, OH, At) cluster models used for benchmarking in Sections D–E.

We also present the results for the long-range corrected version of PBE0, LRC-ωPBEh.[76] This approximation uses a fraction of Hartree–Fock exchange in the short range and transitions to 100% Hartree–Fock exchange in the long range, thus recovering the correct asymptotic behaviour and minimising the delocalisation error. A related version of this XCF, LC-ωPBE,[77–79] has already been found a promising Ansatz for adjusting the approximation's parameters for heavy-element chemistry.[80] Given that LRC-ωPBEh combines the strengths of both PBE0 and LC-ωPBE, it unsurprisingly yields consistently good results. A popular B88P86[81,82] approximation must be used with caution as its success is only serendipitous.

We rely on cluster models to simulate adsorption sites on gold's most stable (111) surface and estimate the effects of surface relaxation caused by the adsorbed species, non-covalent interactions,

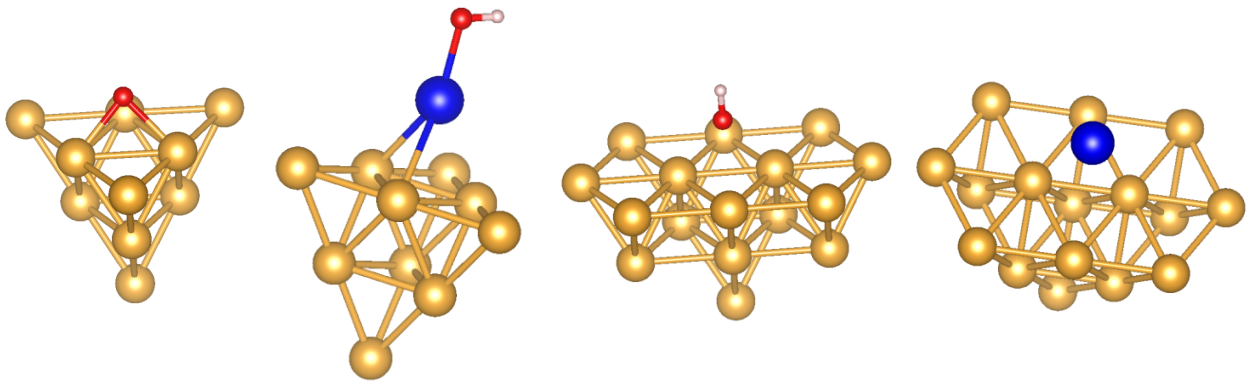

$O - Au_{10}$ hollow-3 | $AtOH - Au_{10}$ hollow-3 | $OH - Au_{16}$ bridge | $At - Au_{16}$ bridge

Figure 2. The types of adsorption complexes considered in the present work. The position of a single adsorbed O atom and the At atom in an adsorbed AtOH molecule is directly above the Au atom in the third layer from the surface ("hollow-3"). The O atom in an adsorbed OH radical and a single adsorbed At atom occupy the bridge position above the middle of chemical bonds of gold atoms of the first layer of the Au(111) surface.

and finite-size effects. To minimise basis-set errors and isolate them from those of the exchange-correlation functional (XCF) approximations, we rely on sufficiently large DFT-specific basis sets: polarisation-consistent aug-pcseg-2 sets for H and O[83] and bespoke in-house sets for At and Au developed for the chosen RECP model. The At basis set is PSO-Lc+g comprised of the large PSO-Lc[84] basis with the g-function from def2-QZVP.[85] For Au, we use the RDFT+g basis made of RDFT[25] and the g-function from def2-QZVP,[85] the original RDFT[25] basis, and RDFT−p, which is the RDFT[25] basis without the most diffuse p-function. We choose the At and Au basis sets depending on the cluster size to keep the computation time reasonable and avoid linear dependencies and the ensuing convergence problems. Because PSO-type basis sets for Tl and Nh are not available yet, in Sec. A, we resort to using uncontracted RDFT-specific basis sets developed in refs. 25,59 and available online.[86] To bring these basis sets to the same formal composition as the At one, we expand both sets with an extra g-function. These functions are taken from the def2-QZVP[85] basis for Tl and E113:GVTZ one for Nh.[86] These sets are also available in ESI.

To quantify the basis-set error and to decide upon the importance of the counterpoise correction in RDFT calculations, we apply the standard Boys–Bernardi procedure[87] and evaluate the basis-set superposition error (BSSE) at the PBE0 level for $AtAu_4$ and OAu_4 cluster models (Fig. 1)

fragmented into Au_4 and the adatom, and for the AtOH molecule fragmented into At and OH. The largest BSSE is found for OAu_4 with the smallest RDFT−p basis for Au, where its value is $-4.98 \cdot 10^{-4}$ a.u., or −1.3 kJ/mol. Given that 1.3 kJ/mol is only 0.31 kcal/mol, which is below the "chemical accuracy" threshold of 1 kcal/mol, the basis sets used in RDFT calculations are virtually complete for the purpose of this work. Therefore, we find it appropriate to consider BSSE only as part of the uncertainty evaluation in Sec. IV.

To minimise the cluster model's finite-size effects on the adsorption energies, we perform a series of calculations with gold clusters progressively increasing from 10 to 69 atoms. These clusters represent the most stable (111) gold surface with Au–Au distances kept at their experimental values for the $Fm\bar{3}m$ crystal structure. We calculate X−Au_n binding energies $E_b(\mathrm{X}-\mathrm{Au_n})$ as

$$-E_b(\mathrm{X}-\mathrm{Au_n}) = E(\mathrm{X}-\mathrm{Au_n}) - E(\mathrm{X}) - E(\mathrm{Au_n}), \tag{1}$$

where $E(\mathrm{X})$ is the energy of the adatom or the isolated molecular adsorbate taken at its equilibrium geometry, $E(\mathrm{Au_n})$ is the energy of the fixed Au_n cluster, and $E_b(\mathrm{X}-\mathrm{Au_n})$ is the energy of the adduct optimised with the Au_n geometry frozen. To ensure reliable convergence of the binding energies with respect to the cluster size, we additionally monitor the net Bader charge[88,89] on the adsorbate (*cf.* ref. 25). The reliability and accuracy of the computational procedure employed in the present work were previously demonstrated in refs. 33,90. In the discussion section, we report binding energies, equilibrium distances between adsorbates and the surface layer of gold clusters, and Bader charges as a function of the inverse cluster size, which we define as $\frac{1}{n^{1/3}}$, where n is the number of Au atoms in the cluster model. Given the size of the largest clusters in these progressions, we use a smaller RDFT−p basis set for Au.

Santiago-Rodriguez *et al.*[91] found that the tetrahedral threefold hollow ("hollow-3") adsorption position is preferable energetically for O atoms on the Au (111) surface. At the same time, the bridge one is only slightly more preferable for OH groups. According to Demidov and Zaitsevskii,[35] the bridge position delivers the global minimum for an At atom adsorbed on

the Au(111) surface, although the energy difference from the "hollow-3" local minimum is insignificant. In the same work,[35] they found the lateral position of the AtOH molecules above the Au(111) surface with the astatine atom located in the "hollow-3" site to be the most stable. We illustrate these optimal positions in Fig. 2 and use them throughout this work.

Our final results for the adsorption energies, which are summarised in Table 6, include zero-point energies (ZPE). The harmonic frequencies required for the ZPE evaluation are calculated using the same cluster models as the underlying electronic structure calculations. In Table 6, we single out the new frequency that results from the formation of the chemical bond between an adsorbate and the Au(111) surface and gives rise to the leading contribution to ZPE correction to the binding. However, all vibrational frequencies are used in the ZPE evaluation.

To quantify the role of non-covalent forces in At and AtOH, as well as O and OH interactions with a gold surface, we use the DFT-D3(BJ)[92] and DFT-D4[93,94] dispersion-correction schemes from the Grimme group, as implemented in TURBOMOLE for standard XCFs, such as PBE0. For the LRC-ωPBEh functional, we employ user-defined D4 parameters from ref. 95. Because of the rapid decay of dispersion interaction with the interatomic distance, we found it sufficient to use an Au_{10} cluster to evaluate their contribution to adsorption energy on Au(111). These corrections, calculated using RDFT Au and PSO-Lc+g At basis sets, are given in Table 2.

To estimate the surface-relaxation effect on the adsorption energy, we choose a model based on the Au_4 cluster, as shown in Fig. 1. Because the equilibrium interatomic distances in an Au_4 cluster significantly differ from those in solid gold, we isolate the relaxation effects caused by the adsorbate as follows. First, we apply constraints to find the (locally) optimal tetrahedral Au_4 geometry and its energy to serve as $E(\mathrm{Au_n})$ in Eq. 1. Then, with an adsorbate X added, we perform two optimisation calculations: one with Au_4 kept frozen at its previous geometry and only the adsorbate's coordinates relaxed, and another with Au_4 relaxed as well while preserving its pyramidal shape. The difference in the resulting $E(\mathrm{X-Au_4})$ values yield adsorbate-specific relaxation effects on Au_4. We summarise the results obtained with PBE0-D3(BJ) and RDFT+g (Au), PSO-Lc+g (At), and aug-pcseg-2 (H, O) basis sets in Table 4 and analyse them in Secs. B–E.

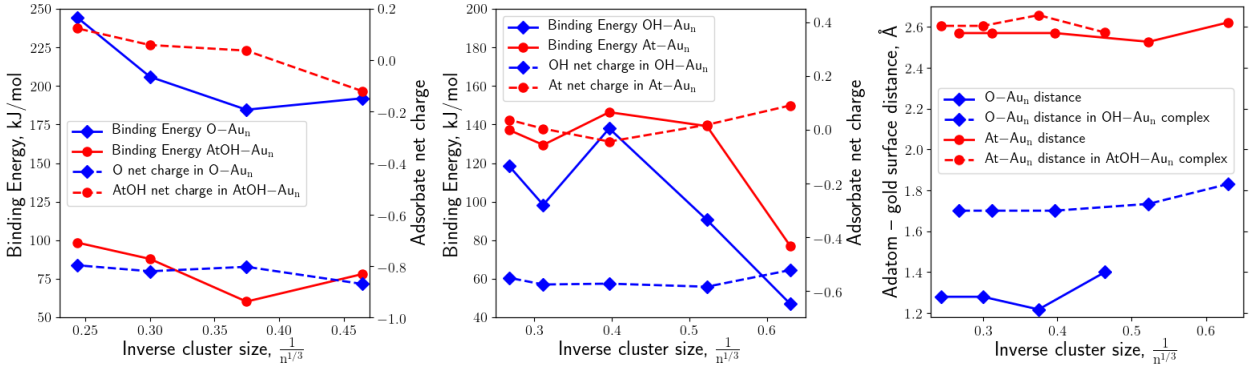

(a) Binding energies and the Bader net charges for adsorbates in hollow-3 position.

(b) Binding energies and the Bader net charges for adsorbates in the bridge position.

(c) Equilibrium distances between adsorbates and the surface layer of the gold clusters for both hollow-3 and bridge adsorption sites.

Figure 3. Binding energies, the Bader net charges, and equilibrium distances of adsorbates with the gold clusters of various sizes. All values are calculated with the 2c-RDFT/PBE0/RDFT−p (Au), PSO-Lc+g (At), aug-pcseg-2 (H, O) approach.

III Results and discussion

In this section, we discuss the properties of adsorbates and our estimates of their adsorption energies in the context of available theoretical and experimental data. Based on these results, we offer a plausible explanation of the outcomes of the recent thermochromatographic experiments.

A Electronic structure and chemical reactivity of the TlOH, AtOH and NhOH molecules

The comparison of the first excitation (1st EE) and the OH-group elimination (D_0) energies for AtOH in Table 3 allows us to surmise that this closed-shell molecule's "promotion" to a reactive triplet-like state, in which it can form a chemical bond, is achievable without dissociation. The NhOH molecule's D_0 is very close to that of AtOH. Still, its 1st EE is 85 kJ/mol higher, suggesting its lower reactivity and, consequently, higher volatility and potential tendency to physisorb on a

Table 2: Dispersion corrections ΔD3(BJ) and ΔD4 to binding energies (in kJ/mol) of At, AtOH, OH, and O with the Au_{10} cluster calculated. ΔD3(BJ) is evaluated with PBE0, and ΔD4 with PBE0 and LRC-ωPBEh, all using RDFT (Au), PSO-Lc+g (At), and aug-pcseg-2 (H, O) basis sets.

	PBE0	PBE0-D3(BJ)	ΔD3(BJ)
At	178	206	28
AtOH	77	107	29
OH	170	182	12
O	192	201	9
	PBE0	PBE0-D4	ΔD4
At	178	205	27
AtOH	78	106	28
OH	170	183	13
O	192	203	11
	LRC-ωPBEh	LRC-ωPBEh-D4	ΔD4
At	172	202	34
AtOH	69	93	24
OH	184	198	14
O	208	220	12

gold surface. The TlOH molecular properties are in stark contrast to those of AtOH and NhOH in much larger 1st EE and D_0, indicative of its chemical inertness and the likely capacity for physisorption only. Interestingly, unlike AtOH and TlOH, 1st EE of NhOH lies in a relatively convenient optical range (*ca.* 21000 cm^{-1}), and it is, in principle, possible to detect these molecules adsorbed on a surface through laser spectroscopy.

Finally, the juxtaposition of 2c-CCSD(T) and RDFT data further validates PBE0 and LRC-ωPBEh accuracy for AtOH and adequacy for TlOH, especially in combination with the D4 dispersion correction. A somewhat inferior agreement for NhOH may be offset by the D4 correction when it becomes available.

B Adsorption of atomic oxygen

Our 2c-RDFT/PBE0 computations with RDFT−p (Au) and aug-pcseg-2 (O) basis sets give the following results. The equilibrium distance between the gold surface and the O atom, which we put in the preferred hollow-3 position,[91] varies in the 1.21–1.40 Å range and stabilises at $R_e = 1.28$ Å in $O - Au_{37}$ and $O - Au_{69}$ adsorption complexes (see Figure 3c for details). The corresponding

Table 3: Excitation energies to the first excited open-shell state (1st EE, kJ/mol) for TlOH, AtOH, NhOH monohydroxides calculated at the FS RCCSD level and their hydroxyl group elimination energies D_0 (kJ/mol), obtained at the relativistic 2c-CCSD(T) (with counterpoise correction) and 2c-RDFT levels. The D4 correction to DFT energies is given in square brackets when available. Optimal geometries are taken from ref. 33. Hydroxyl group elimination energies include ZPE contributions[33] (6 kJ/mol for TlOH and AtOH, 7 kJ/mol for NhOH). The BSSE contributions are given in parentheses.

		D_0				
Molecule	1st EE	2c-CCSD(T)	CCSD(T)+Δ_{SO}[33]	PBE0	LRC-ωPBEh	Exptl.[96]
TlOH	340	313(−13)	319	299[+3]	297[+4]	330±30
AtOH	163	167(−10)	174	164[+3]	160[+4]	–
NhOH	248	170(−1)	188	156	150	–

equilibrium distance between O and the nearest gold atom is 2.10 Å. For all cluster model sizes studied, the Bader charge on the O adatom is negative and converges to $O^{-0.8}$. The binding energies for $O-Au_{37}$ and $O-Au_{69}$ complexes equal to 206 kJ/mol and 244 kJ/mol, respectively.

The D4 correction to the binding energy is 11 kJ/mol (Table 2) and ZPE contribution −8 kJ/mol added to 244 kJ/mol for $O-Au_{69}$ bring our final estimate of the $O-Au(111)$ adsorption energy to 247 kJ/mol. This result agrees with the 234 ± 33 kJ/mol experimental value[97] reasonably well. The calculated vibrational frequency of the $O-Au\,(111)$ stretch on the hollow-3 site is 427 cm^{-1}, which differs from the experimental result[98] (380 cm^{-1}) by less than 50 cm^{-1}.

C Adsorption of OH radicals

The chemistries of hydroxyl radicals and atomic halogens bear some similarities,[99] thus making it conceivable to benchmark the adsorption of elemental atomic At on the Au(111) surface against that of OH.

We first consider the properties of the $Au-OH$ bond in molecular gold hydroxide. Our 2c-RDFT/PBE0 estimate using RDFT (Au) and aug-pcseg-2 (H, O) basis sets for hydroxyl group elimination energy for AuOH is 207 kJ/mol, which agrees with a previously reported advanced result of 195 kJ/mol[100] reasonably well. Interestingly, the latter value is quite close to D_e(AtAu) = 186 kJ/mol,[37] supporting the hypothesis that At and OH behave similarly in their interaction

with gold. The Bader net charge distribution in an AuOH molecule is $Au^{+0.40}O^{-0.98}H^{+0.59}$, corresponding to a -0.40 charge transfer from Au to OH.

According to ref. 91, the preferred adsorption site for isolated hydroxyl groups is the bridge. Starting from the Au_{16} cluster (the inverse cluster size $\frac{1}{n^{1/3}} = 0.397$), we find that the equilibrium distance between the gold surface and the O atom varies slightly with the size of the cluster model and stabilises at $R_e = 1.70$ Å (see Figure 3c for details). This value corresponds to the equilibrium distance of 2.23 Å between O and the nearest gold atom. As expected, the Bader charge on the OH moiety is negative for all cluster model sizes; it stabilises at -0.57. Our converged 2c-RDFT/PBE0 (RDFT$-$p (Au) and aug-pcseg-2 (H, O) basis sets) estimate of the $OH - Au_n$ binding energy equals 118 kJ/mol. Adding the D4 correction (11 kJ/mol from Table 2) and ZPE contribution (-12 kJ/mol), we estimate the isolated hydroxyl group adsorption energy on the Au(111) surface to be 119 kJ/mol. The calculated vibrational frequencies of the OH – Au(111) stretch on the bridge site and the stretching mode of the adsorbed OH group are 317 and 3885 cm^{-1}, respectively. The latter frequency agrees with the experimental value[101] of 3750 cm^{-1}.

D Adsorption of atomic astatine

To address significant discrepancies in theoretical At–Au(111) binding energies estimates[35,36,38] attributed by Ryzhkov *et al.*[38] to possible shortcomings of the cluster model used in ref. 35, we first consider the potential effects of Au(111) relaxation. To this end, we calculate the At–Au_4 binding energies, $E_b(At - Au_4)$ using the 2c-RDFT/PBE0-D3(BJ) and 2c-RDFT/PBE0-D4 approach outlined in Section C. As shown in Table 4, the Au_4 relaxation effect on $E_b(At - Au_4)$/2c-RDFT/PBE0-D3(BJ) is 3.6 kJ/mol. Given that $E_b(At - Au_4) = 188$ kJ/mol, this effect is negligible.

We apply the same scheme to estimate the relaxation effect for other adsorbates: AtOH, O, and OH. Our results, also presented in Table 4, indicate that only the largest effects observed in O and OH adsorption rise above the "chemical accuracy" threshold of 1 kcal/mol ever so slightly, while for AtOH, the effect practically vanishes. Based on these estimates, we find it reasonable to

Table 4: Binding energies (in kJ/mol) of At and O species with the Au_4 cluster and the cluster relaxation effects calculated at the PBE0-D3(BJ) level with RDFT+g (Au), PSO-Lc+g (At), and aug-pcseg-2 (H, O) basis sets. PBE0-D4 predicts indistinguishable results, which appear in parentheses.

Adsorbate	Au_n frozen	Au_n relaxed	Relaxation effect
At	184.1 (183.6)	187.7 (187.1)	3.6 (3.5)
AtOH	119.6 (119.4)	120.9 (120.6)	1.2 (1.2)
O	210.1 (211.1)	219.3 (220.4)	9.2 (9.3)
OH	131.8 (132.4)	139.2 (139.8)	7.3 (7.4)

consider relaxation effects solely as part of the results' uncertainty estimate in Sec. IV.

Previous calculations[35] indicate that the At atom's preferable binding site on the Au (111) surface is the bridge position. From Au_{16} on, i.e., for $\frac{1}{n^{1/3}} \leq 0.398$, the equilibrium distance between the gold surface and the At atom varies only slightly with the cluster size, as illustrated in Figure 3c. It stabilises at $R_e = 2.57$ Å, corresponding to the equilibrium distance of 2.95 Å between At and the nearest gold atom. For Au_7 ($\frac{1}{n^{1/3}} = 0.523$) and larger clusters, the net Bader charge on the At atom practically disappears, indicating that the At–Au(111) adsorption does not involve charge transfer. The 2c-RDFT/PBE0 estimate of the $At - Au_{52}$ complex binding energy is 137 kJ/mol, which agrees with the earlier estimate of 130 ± 10 kJ/mol[35] quite well. With the D4 correction (+27 kJ/mol) added from Table 2 and ZPE contribution (−7 kJ/mol), the final value becomes 157 kJ/mol. This theoretical result is in excellent agreement with the experimental estimate of 147 ± 15 kJ/mol.[40] The calculated frequency of the At – Au(111) stretch vibrational mode at the bridge site is 122 cm^{-1}.

The final $E_b(\mathrm{At} - \mathrm{Au}(111))$ = 157 kJ/mol value is smaller than $E_b(\mathrm{At} - \mathrm{Au}_4)$ = 188 kJ/mol in the At–Au_4 model employed at the beginning of this section to evaluate the effect of adsorption-induced Au(111) relaxation. This observation allows us to infer that the actual At–Au(111) interaction is even less capable of causing meaningful relaxation effects. The dispersion correction to $E_b(\mathrm{At} - \mathrm{Au}(111))$ is indeed found to be significant. However, its inclusion in the present work further justifies the validity of our cluster model instead of revealing its purported "obvious limitations,"[38] especially in light of the available experimental data.[40]

E Adsorption of AtOH molecules

Relative to the At–Au(111) case, the discrepancies in the available theoretical estimates of AtOH–Au(111) adsorption energies are even more significant,[35,38] with At–Au(111) and AtOH–Au(111) binding energies being virtually indistinguishable in ref. 38. As with At–Au(111), Ryzhkov *et al.*[38] also attribute the stark contrast between their $E_b(\mathrm{AtOH-Au(111)})$ = 189 kJ/mol and 90±10 kJ/mol by Demidov and Zaitsevskii[35] to the deficiencies of the cluster model employed in the latter work. To revisit this controversy, especially in light of the newest experimental data,[32] we first apply the smallest Au_4 cluster model and summarise the results in Table 5.

Table 5: Binding energies (in kJ/mol) of At with the Au_4 cluster. These energies include the effects of Au_4 relaxation.

System	PBE0-D4	LRC-ωPBEh-D4
At–Au_4	187.1	176.3
AtOH–Au_4	120.6	104.0
$^{\mathrm{AtOH}}\Delta^{\mathrm{At}}$	66.5	72.3

The 2c-RDFT/PBE0-D4 AtOH–Au_4 binding energy is 120.6 kJ/mol, which is $^{\mathrm{AtOH}}\Delta^{\mathrm{At}}$ = 66.5 kJ/mol smaller than 187.1 kJ/mol for At–Au_4, where both energies include the Au_4 cluster relaxation. Analogous LRC-ωPBEh-D4 calculations give a similar result (see Table 5). As outlined in the previous section for atomic At, surface-relaxation effects are minuscule. They cannot compromise the ability of the cluster model to elucidate marked differences in At and AtOH interactions with Au(111).

The 2c-RDFT/PBE0 binding energy of the AtOH molecule (in the preferred lateral position, see Fig. 2) with the Au_{69} gold cluster is 98 kJ/mol and becomes 117 kJ/mol with the D4 (+28 kJ/mol) and ZPE (−9 kJ/mol) corrections added to it. This value is in good agreement with the experimental result 100^{+20}_{-10} kJ/mol[40] and compatible with the detection of a volatile species, most likely AtOH, with the adsorption energy's lower bound estimated at 90 kJ/mol.[32] In this adsorption position, the astatine atom is located at the hollow-3 site, with the equilibrium distance from the surface layer of gold equal to 2.61 Å (see Figure 3c for details). In all cluster models, AtOH binding with the Au(111) surface remains consistently and meaningfully weaker than that

of atomic At with $^{\mathrm{AtOH}}\Delta^{\mathrm{At}}$ stabilising at *ca.* 40 kJ/mol.

The $\mathrm{At}-\mathrm{O}$ bond length in the $\mathrm{AtOH}-\mathrm{Au_n}$ adsorption complex (2.18 Å) is only slightly larger than in the isolated AtOH molecule (2.13 Å). In the adsorbed state, our estimates of the At – OH bending and stretching modes are 828 cm^{-1} and 358 cm^{-1}, respectively. These values are red-shifted by *ca.* 160 cm^{-1} relative to the same modes in the isolated AtOH molecule[33] (985 cm^{-1} and 519 cm^{-1}, respectively). The O–H stretching mode in the adsorbed AtOH molecule (3850 cm^{-1}) remains the same as in isolated AtOH. Therefore, it is reasonable to conclude that the adsorption of AtOH on the Au(111) surface does not cause the At–O bond dissociation. In contrast, such dissociation can be inferred from Fig. 6 in ref. 38 (see ESI for the logic behind this inference).

F Reactions on a gold surface

The mechanism of AtOH formation in thermochromatographic experiments remains to be established. However, heterogeneous chemical reactions can occur even on gold's most stable Au(111) surface. For example, previous studies[102,103] demonstrate that hydroxyl groups adsorbed on the Au (111) surface are unstable via the recombination reaction 2:

$$2\mathrm{OH_{ads}} \rightarrow \mathrm{O_{ads}} + \mathrm{H_2O}. \tag{2}$$

This reaction is noticeably exothermic: our 2c-RDFT/PBE0-D4 estimate gives $E_{\mathrm{rxn}} = -58$ kJ/mol. This reaction is practically irreversible if the gas flow immediately carries the water molecules away from the surface.

Our re-evaluation of the At, AtOH, O, and OH interactions with the Au(111) surface has led us to propose the following explanation of the AtOH formation when At atoms and OH radicals are simultaneously present in the carrier gas. The adsorption energy of At atoms (157 kJ/mol) exceeds that of OH groups (119 kJ/mol). Thus, in a thermochromatographic experiment, At atoms adsorb on a gold surface at a higher temperature and before OH radicals. However, the OH radical

adsorption energy (119 kJ/mol) is close to our estimate of the OH group elimination energy from adsorbed AtOH, which is 127 kJ/mol in the AtOH$-$Au$_{69}$/2c-RDFT/PBE0-D4-ZPE adsorption complex model. Therefore, it is conceivable that the adsorbed At atoms act as precursors to the formation of AtOH molecules:

$$\mathrm{At_{ads}} + \mathrm{OH} \rightarrow \mathrm{AtOH}. \tag{3}$$

According to our 2c-RDFT/PBE0-D4-ZPE model, reaction 3 proceeds almost isoenergetically: $E_{\mathrm{rxn}} = -3$ kJ/mol. Of all species involved (except for H_2O, whose adsorption energy on the Au(111) surface is about 14.5 kJ/mol[104]), AtOH molecules are most volatile as they require the lowest energy to desorb from the gold surface. If we hypothesise their formation via reaction 3 at the temperature of At atoms' adsorption, these AtOH molecules will immediately desorb from the gold surface. They can re-adsorb further down the thermochromatographic column at lower temperatures, thus explaining the detection of a volatile species in refs. 32,40.

IV Conclusions

We present an exhaustive theoretical study of At and AtOH in light of the outcomes of the most recent thermochromatographic experiments on a gold surface and in the context of revealing the chemical homology of superheavy elements. Our relativistic coupled-cluster investigation into the electronic structure of TlOH, AtOH, and NhOH demonstrates that while Tl and Nh are Group 13 elements, the energy gaps between the ground and first excited states of these molecules — 340 kJ/mol in TlOH, 163 kJ/mol in AtOH, and 248 kJ/mol in NhOH — suggest chemical reactivity of NhOH is closer to that of AtOH than TlOH. The OH group elimination energies — 313, 167, and 170 kJ/mol for, respectively, TlOH, AtOH, and NhOH — indicate that chemical homology between Nh and At is much more plausible than between Nh and Tl.

Considering the potential of At as a chemical homologue of Nh and the preparations for future Nh detection and chemical characterisation, we have employed a meticulously assessed relativistic

DFT approach to model the behaviour of the species in thermochromatographic experiments with astatine on the Au(111) surface with a high degree of precision. Our revised estimates of O, OH, At, and AtOH adsorption energies on the Au(111) surface are 247 kJ/mol, 119 kJ/mol, 157 kJ/mol, and 117 kJ/mol, respectively. The sources of our 2c-RDFT/PBE0-D4-ZPE results' uncertainty include the choice of the exchange-correlation functional (up to 15 kJ/mol between PBE0 and LRC-ωPBEh), cluster-relaxation effects (less than 4 kJ/mol), and the basis set superposition error (about 1 kJ/mol). Therefore, we can reasonably ascribe a $\pm$10 kJ/mol uncertainty range to our theoretical data. These values agree with the values derived from the experimental data:[40,97] 234 ± 33 kJ/mol for O, 147 ± 15 kJ/mol for At, and 100^{+20}_{-10} kJ/mol for AtOH, thus corroborating the correctness of our results and the viability of the quantum-chemical approaches employed. Most notably, we confirm that the adsorption energy of AtOH on the Au(111) surface is significantly lower than that of At (by *ca.* 40 kJ/mol), contrary to the most recent theoretical study.[38] Our model of O, OH, At, and AtOH interaction with Au(111) allows us to propose a heterogeneous reaction on the gold surface responsible for the formation of the experimentally detected AtOH and set the stage for predicting the behaviour of superheavy elements in thermochromatographic experiments.

Author Contributions

The authors contributed equally.

Conflicts of interest

There are no conflicts to declare.

Acknowledgements

We thank Prof. Christoph van Wüllen for providing the relativistic DFT code and Drs. Andréi Zaitsevskii and Anatoly Titov for helpful discussions. A.A.R. thanks Dr. Uwe Huniar for promptly addressing several important issues in the TURBOMOLE programme and the Biomedical Research Center at Oakland University for support through the Research Excellence Program. High-performance computing facilities at Oakland University were provided via collaboration between the Oakland University Research Office and University Technology Services.

References

(1) Oganessian, Y. Heaviest Nuclei from ^{48}Ca-induced Reactions. *J. Phys. Conf. Ser.* **2011**, *312*, 082003.

(2) Holmbeck, E. M.; Barnes, J.; Lund, K. A.; Sprouse, T. M.; McLaughlin, G. C.; Mumpower, M. R. Superheavy Elements in Kilonovae. *Astrophys. J. Lett.* **2023**, *951*, L13.

(3) Holmbeck, E. M.; Sprouse, T. M.; Mumpower, M. R. Nucleosynthesis and observation of the heaviest elements. *Eur. Phys. J. A* **2023**, *59*, 28.

(4) Haba, H. A new period in superheavy-element hunting. *Nat. Chem.* **2019**, *11*, 10–13.

(5) Smits, O. R.; Düllmann, C. E.; Indelicato, P.; Nazarewicz, W.; Schwerdtfeger, P. The quest for superheavy elements and the limit of the periodic table. *Nat. Rev. Phys.* **2024**, *6*, 86–98.

(6) Pyykkö, P. Is the Periodic Table all right ("PT OK")? *EPJ Web of Conferences* **2016**, *131*, 01001.

(7) Karol, P. J. Elements Old and New: Discoveries, Developments, Challenges, and Environmental Implications. *ACS Symp. Ser.* **2017**, 41–66.

(8) Giuliani, S. A.; Matheson, Z.; Nazarewicz, W.; Olsen, E.; Reinhard, P.-G.; Sadhukhan, J.; Schuetrumpf, B.; Schunck, N.; Schwerdtfeger, P. Colloquium: Superheavy elements: Oganesson and beyond. *Rev. Mod. Phys.* **2019**, *91*, 011001.

(9) Pershina, V. Relativity in the electronic structure of the heaviest elements and its influence on periodicities in properties. *Radiochim. Acta* **2019**, *107*, 833–863.

(10) Schwerdtfeger, P.; Smits, O. R.; Pyykkö, P. The periodic table and the physics that drives it. *Nat. Rev. Chem.* **2020**, *4*, 359–380.

(11) Eichler, R. et al. Chemical characterization of element 112. *Nature* **2007**, *447*, 72–75.

(12) Eichler, R.; Aksenov, N. V.; Albin, Y. V.; Belozerov, A. V.; Bozhikov, G. A.; Chepigin, V. I.; Dmitriev, S. N.; Dressler, R.; Gaeggeler, H. W.; Gorshkov, V. A.; Henderson, G. Indication for a volatile element 114. *Radiochim. Acta* **2010**, *98*, 133–139.

(13) Yakushev, A. et al. Superheavy element flerovium (element 114) is a volatile metal. *Inorg. Chem.* **2014**, *53*, 1624–1629.

(14) Aksenov, N. V. et al. On the volatility of nihonium (Nh, Z = 113). *Eur. Phys. J. A* **2017**, *53*, 1–5.

(15) Karol, P. J.; Barber, R. C.; Sherrill, B. M.; Vardaci, E.; Yamazaki, T. Discovery of the elements with atomic numbers Z= 113, 115 and 117 (IUPAC Technical Report). *Pure Appl. Chem.* **2016**, *88*, 139–153.

(16) Zvára, I. *Experimental Developments in Gas-Phase Radiochemistry*; Springer, 2008; pp 1–225.

(17) Schwerdtfeger, P.; Smits, O. R.; Pyykkö, P. The Periodic table and the physics that drives it. *Nat. Rev. Chem.* **2020**, *4*, 359–380.

(18) Cao, C.; Vernon, E., René; Schwarz, W. H. E.; Li, J. Understanding Periodic and Non-periodic Chemistry in Periodic Tables. *Front. Chem.* **2021**, *8*, 813.

(19) Türler, A.; Eichler, R.; Yakushev, A. Chemical studies of elements with Z¿ 104 in gas phase. *Nucl. Phys. A* **2015**, *944*, 640–689.

(20) Bagus, P. S.; Suzer, S. 6p valence relativistic effects in 5d photoemission spectrum of Pb atom and bonding properties of Pb-dimer using Dirac–Hartree–Fock formalism including many-body effects. *J. Vac. Sci. Technol. A: Vac., Surf., Films* **2022**, *40*, 043205.

(21) Toyoshima, A.; Mitsukai, A.; Tsukada, K.; Ooe, K.; Haba, H.; Komori, Y.; Murakami, M.; Kaneya, Y.; Sato, D.; Asai, M.; Sato, T. K.; Nagame, Y. Extraction behavior of Mo and W from H2SO4 and HF/HCl solutions into toluene with Aliquat336: sulfate and fluoride complex formation of Mo and W towards chemical studies of seaborgium (Sg). *J. Radioanal. Nucl. Chem.* **2018**, *317*, 421–430.

(22) Bartl, P.; Němec, M.; Zach, V.; Bulíková, A.; Šifnerová, L.; Štursa, J.; Omtvedt, J.; John, J. Fast on-line dissolution of KCl aerosol particulates for liquid-phase chemistry with homologues of superheavy elements. *Nucl. Instrum. Methods Phys. Res., Sect. A* **2023**, *1055*, 168500.

(23) Attallah, M. F.; Elchine, D.; Grödler, D.; Margreiter, R.; Maslo, M.; Michel, M.; Omtvedt, J. P.; Strub, E.; Döllen, S. v. Trace-scale extraction of carrier-free tungsten radioisotope as a homolog of Sg using ionic liquid from acid solutions: Kinetic study. *Sep. Purif. Technol.* **2024**, *331*, 125418.

(24) Yakushev, A. et al. First Study on Nihonium (Nh, Element 113) Chemistry at TASCA. *Front. Chem.* **2021**, *9*, 753738.

(25) Rusakov, A. A.; Demidov, Y. A.; Zaitsevskii, A. Estimating the adsorption energy of element 113 on a gold surface. *Cent. Eur. J. Phys.* **2013**, *11*, 1537–1540.

(26) Serov, A.; Eichler, R.; Dressler, R.; Piguet, D.; Türler, A.; Vögele, A.; Wittwer, D.; Gäggeler, H. W. Adsorption interaction of carrier-free thallium species with gold and quartz surfaces. *Radiochim. Acta* **2013**, *101*, 421–426.

(27) Zaitsevskii, A. V.; Rykova, E. A.; Titov, A. V. Theoretical studies on the structures and properties of superheavy element compounds. *Russ. Chem. Rev.* **2008**, *77*, 205.

(28) Demidov, Y. A.; Zaitsevskii, A. Simulation of chemical properties of superheavy elements from the island of stability. *Russ. Chem. Bull.* **2014**, *63*, 1647–1655.

(29) White, H. E. Pictorial Representations of the Dirac Electron Cloud for Hydrogen-Like Atoms. *Physical Review* **1931**, *38*, 513–520.

(30) Szabo, A. Contour diagrams for relativistic orbitals. *J. Chem. Educ.* **1969**, *46*, 678.

(31) Hatano, Y.; Yamamoto, S.; Tatewaki, H. Visualization of the Exact Solution of Dirac Equation. *J. Comp. Chem. Japan* **2016**, *15*, 2016–0014.

(32) Chiera, N. M. et al. Observation of a volatile astatine hydroxide species in online gas-adsorption thermochromatography experiments. *Mol. Phys.* **2023**, *ahead-of-print*, e2272685.

(33) Demidov, Y.; Zaitsevskii, A. A comparative study of molecular hydroxides of element 113 (I) and its possible analogs: *Ab initio* electronic structure calculations. *Chem. Phys. Lett.* **2015**, *638*, 21 – 24.

(34) Demidov, Y. A.; Zaitsevskii, A. Chemical Pseudo-Homologues of Superheavy Element 113. Proceedings of International Symposium on Exotic Nuclei. 2015; pp 285–290.

(35) Demidov, Y.; Zaitsevskii, A. Adsorption of the astatine species on a gold surface: A relativistic density functional theory study. *Chem. Phys. Lett.* **2018**, *691*, 126–130.

(36) Tanudji, J.; Aspera, S. M.; Kasai, H.; Okada, M.; Ogawa, T.; Nakanishi, H. Computational Nanomaterials Design: towards the Realization of Nanoparticle use in Radiotherapy Case Study 2: Adsorption states of At on Au (111) Surface. *Phys. Sci. Int. J.* **2022**, *26*, 1–10.

(37) Casetti, V. T.; MacLean, J.; Ayoub, A. D.; Fredericks, R. J.; Adamski, J. A.; Rusakov, A. A. Investigating the Heaviest Halogen: Lessons Learned from Modeling the Electronic Structure of Astatine's Small Molecules. *J. Phys. Chem. A* **2022**, *127*, 46–56.

(38) Ryzhkov, A.; Pershina, V.; Iliaš, M.; Shabaev, V. A theoretical study of the adsorption behavior of superheavy 7p-elements and their compounds on a surface of gold in comparison with their lighter homologs. *Phys. Chem. Chem. Phys.* **2023**, *25*, 15362–15370.

(39) Trombach, L.; Ehlert, S.; Grimme, S.; Schwerdtfeger, P.; Mewes, J.-M. Exploring the chemical nature of super-heavy main-group elements by means of efficient plane-wave density-functional theory. *Phys. Chem. Chem. Phys.* **2019**, *21*, 18048–18058.

(40) Serov, A.; Aksenov, N.; Bozhikov, G.; Eichler, R.; Dressler, R.; Lebedev, V.; Petrushkin, O.; Piguet, D.; Shishkin, S.; Tereshatov, E.; Türler, A.; Voegele, A.; Wittwer, D.; Gäggeler, H. Adsorption interaction of astatine species with quartz and gold surfaces. *Radiochim. Acta* **2011**, *99*, 593–600.

(41) Galland, N.; Montavon, G.; Le Questel, J.-Y.; Graton, J. Quantum calculations of At-mediated halogen bonds: on the influence of relativistic effects. *New J. Chem.* **2018**, *42*, 10510–10517.

(42) Mosyagin, N.; Eliav, E.; Titov, A.; Kaldor, U. Comparison of relativistic effective core potential and all-electron Dirac-Coulomb calculations of mercury transition energies by the relativistic coupled-cluster method. *J. Phys. B: At. Mol. Opt. Phys.* **2000**, *33*, 667.

(43) Oleynichenko, A. V.; Zaitsevskii, A.; Mosyagin, N. S.; Petrov, A. N.; Eliav, E.; Titov, A. V. LIBGRPP: A library for the evaluation of molecular integrals of the generalized relativistic pseudopotential operator over Gaussian functions. *Symmetry* **2023**, *15*, 197.

(44) Mosyagin, N. S.; Zaitsevskii, A.; Titov, A. V. Shape-consistent relativistic effective potentials of small atomic cores. *Int. Rev. At. Mol. Phys.* **2010**, *1*, 63–72.

(45) Mosyagin, N. S.; Zaitsevskii, A. V.; Titov, A. V. Generalized relativistic effective core potentials for superheavy elements. *Int. J. Quantum Chem.* **2020**, *120*, e26076.

(46) Mosyagin, N. S.; Oleynichenko, A. V.; Zaitsevskii, A.; Kudrin, A. V.; Pazyuk, E. A.; Stolyarov, A. V. Ab initio relativistic treatment of the $a^3\Pi - X^1\Sigma^+$, $a'^3\Sigma^+ - X^1\Sigma^+$ and $A^1\Pi - X^1\Sigma^+$ systems of the CO molecule. *J. Quant. Spectrosc. Radiat. Transf.* **2021**, *263*, 107532.

(47) Zaitsevskii, A.; Mosyagin, N. S.; Oleynichenko, A. V.; Eliav, E. Generalized relativistic small-core pseudopotentials accounting for quantum electrodynamic effects: Construction and pilot applications. *Int. J. Quantum Chem.* **2023**, *123*, e27077.

(48) Mulliken, R. S. The assignment of quantum numbers for electrons in molecules. I. *Phys. Rev.* **1928**, *32*, 186.

(49) Kaldor, U. The Fock space coupled cluster method: theory and application. *Theor. Chim. Acta* **1991**, *80*, 427–439.

(50) Visscher, L.; Eliav, E.; Kaldor, U. Formulation and implementation of the relativistic Fock-space coupled cluster method for molecules. *J. Chem. Phys.* **2001**, *115*, 9720–9726.

(51) Eliav, E.; Borschevsky, A.; Zaitsevskii, A.; Oleynichenko, A. V.; Kaldor, U. *Reference Module in Chemistry, Molecular Sciences and Chemical Engineering*; Elsevier, 2022.

(52) Kaldor, U.; Haque, A. Open-shell coupled-cluster method: Direct calculation of excitation energies. *Chem. Phys. Lett.* **1986**, *128*, 45–48.

(53) Musiał, M.; Bartlett, R. J. Fock space multireference coupled cluster method with full inclusion of connected triples for excitation energies. *J. Chem. Phys.* **2004**, *121*, 1670–1675.

(54) Oleynichenko, A. V.; Zaitsevskii, A.; Eliav, E. Towards high performance relativistic electronic structure modelling: the EXP-T program package. Supercomputing. Cham, 2020; pp 375–386, DOI: 10.1007/978-3-030-64616-5_33.

(55) Oleynichenko, A. V.; Rumyantsev, A. S.; Zaitsevskii, A.; Eliav, E. EXP-T, an extensible code for Fock space relativistic coupled cluster calculations, http://www.qchem.pnpi.spb.ru/expt (accessed on 20 July 2024).

(56) DIRAC, a relativistic ab initio electronic structure program, Release DIRAC19 (2019), written by A. S. P. Gomes, T. Saue, L. Visscher, H. J. Aa. Jensen, and R. Bast, with contributions from I. A. Aucar, V. Bakken, K. G. Dyall, S. Dubillard, U. Ekstroem, E. Eliav, T. Enevoldsen, E. Fasshauer, T. Fleig, O. Fossgaard, L. Halbert, E. D. Hedegaard, T. Helgaker, J. Henriksson, M. Ilias, Ch. R. Jacob, S. Knecht, S. Komorovsky, O. Kullie, J. K. Laerdahl, C. V. Larsen, Y. S. Lee, H. S. Nataraj, M. K. Nayak, P. Norman, M. Olejniczak, J. Olsen, J. M. H. Olsen, Y. C. Park, J. K. Pedersen, M. Pernpointner, R. Di Remigio, K. Ruud, P. Salek, B. Schimmelpfennig, B. Senjean, A. Shee, J. Sikkema, A. J. Thorvaldsen, J. Thyssen, J. van Stralen, M. L. Vidal, S. Villaume, O. Visser, T. Winther, and S. Yamamoto (see http://diracprogram.org). (accessed on 3 May 2024).

(57) Saue, T. et al. The DIRAC code for relativistic molecular calculations. *J. Chem. Phys.* **2020**, *152*, 204104.

(58) Peterson, K. A.; Figgen, D.; Goll, E.; Stoll, H.; Dolg, M. Systematically convergent basis sets with relativistic pseudopotentials. II. Small-core pseudopotentials and correlation consistent basis sets for the post-*d* group 16–18 elements. *J. Chem. Phys.* **2003**, *119*, 11113–11123.

(59) Zaitsevskii, A.; Titov, A. V.; Rusakov, A. A.; van Wüllen, C. *Ab initio* study of element 113–gold interactions. *Chem. Phys. Lett.* **2011**, *508*, 329–331.

(60) Basis sets for Tl, At and Nh are given in Supplementary Information.

(61) de Jong, W. A.; Harrison, R. J.; Dixon, D. A. Parallel Douglas–Kroll energy and gradients in NWChem: Estimating scalar relativistic effects using Douglas–Kroll contracted basis sets. *J. Chem. Phys.* **2001**, *114*, 48–53.

(62) Visscher, L.; Lee, T. J.; Dyall, K. G. Formulation and implementation of a relativistic unrestricted coupled-cluster method including noniterative connected triples. *J. Chem. Phys.* **1996**, *105*, 8769–8776.

(63) Aprà, E. et al. NWChem: Past, present, and future. *J. Chem. Phys.* **2020**, *152*, 184102.

(64) Balasubramani, S. G. et al. TURBOMOLE: Modular program suite for ab initio quantum-chemical and condensed-matter simulations. *J. Chem. Phys.* **2020**, *152*, 184107.

(65) Baldes, A.; Weigend, F. Efficient two-component self-consistent field procedures and gradients: implementation in TURBOMOLE and application to Au_{20}^-. *Mol. Phys.* **2013**, *111*, 2617–2624.

(66) van Wüllen, C. A Quasirelativistic Two-component Density Functional and Hartree-Fock Program. *Z. Phys. Chem.* **2010**, *224*, 413–426.

(67) Autschbach, J. Comprehensive Computational Chemistry (First Edition). *Advanced Electronic Structure Methods in Computational Quantum Chemistry* **2024**, 177–192.

(68) Sergentu, D.; David, G.; Montavon, G.; Maurice, R.; Galland, N. Scrutinizing "Invisible" astatine: A challenge for modern density functionals. *Journal of Computational Chemistry* **2016**, *37*, 1345–1354.

(69) Maier, T. M.; Ikabata, Y.; Nakai, H. Relativistic local hybrid functionals and their impact on 1s core orbital energies. *J. Chem. Phys.* **2020**, *152*, 214103.

(70) Rothe, S. et al. Measurement of the first ionization potential of astatine by laser ionization spectroscopy. *Nat. Commun.* **2013**, *4*, 1835.

(71) Leimbach, D. et al. The electron affinity of astatine. *Nat. Commun.* **2020**, *11*, 3824.

(72) Klopper, W.; Bachorz, R. A.; Tew, D. P.; Hättig, C. Sub-meV accuracy in first-principles computations of the ionization potentials and electron affinities of the atoms H to Ne. *Phys. Rev. A* **2010**, *81*, 022503.

(73) Kristiansson, M. K. et al. High-precision electron affinity of oxygen. *Nat. Commun.* **2022**, *13*, 5906.

(74) Adamo, C.; Barone, V. Toward reliable density functional methods without adjustable parameters: The PBE0 model. *J. Chem. Phys.* **1999**, *110*, 6158–6170.

(75) Ernzerhof, M.; Scuseria, G. E. Assessment of the Perdew–Burke–Ernzerhof exchange-correlation functional. *J. Chem. Phys.* **1999**, *110*, 5029–5036.

(76) Rohrdanz, M. A.; Martins, K. M.; Herbert, J. M. A long-range-corrected density functional that performs well for both ground-state properties and time-dependent density functional theory excitation energies, including charge-transfer excited states. *J. Chem. Phys.* **2009**, *130*, 054112.

(77) Vydrov, O. A.; Heyd, J.; Krukau, A. V.; Scuseria, G. E. Importance of short-range versus long-range Hartree-Fock exchange for the performance of hybrid density functionals. *J. Chem. Phys.* **2006**, *125*, 074106.

(78) Vydrov, O. A.; Scuseria, G. E. Assessment of a long-range corrected hybrid functional. *J. Chem. Phys.* **2006**, *125*, 234109.

(79) Henderson, T. M.; Janesko, B. G.; Scuseria, G. E. Generalized gradient approximation model exchange holes for range-separated hybrids. *J. Chem. Phys.* **2008**, *128*, 194105.

(80) Duignan, T. J.; Autschbach, J.; Batista, E.; Yang, P. Assessment of Tuned Range Separated Exchange Functionals for Spectroscopies and Properties of Uranium Complexes. *J. Chem. Theory Comput.* **2017**, *13*, 3614–3625.

(81) Becke, A. D. Density-functional exchange-energy approximation with correct asymptotic behavior. *Phys. Rev. A* **1988**, *38*, 3098–3100.

(82) Perdew, J. P. Density-functional approximation for the correlation energy of the inhomogeneous electron gas. *Phys. Rev. B* **1986**, *33*, 8822–8824.

(83) Jensen, F. Unifying general and segmented contracted basis sets. Segmented polarization consistent basis sets. *J. Chem. Theory Comput.* **2014**, *10*, 1074–1085.

(84) Espinosa, K. J. R.; Kananenka, A. A.; Rusakov, A. A. Novel Computational Chemistry Infrastructure for Simulating Astatide in Water: From Basis Sets to Force Fields Using Particle Swarm Optimization. *J. Chem. Theory Comput.* **2023**, *19*, 7998–8012.

(85) Weigend, F.; Ahlrichs, R. Balanced basis sets of split valence, triple zeta valence and quadruple zeta valence quality for H to Rn: Design and assessment of accuracy. *Phys. Chem. Chem. Phys.* **2005**, *7*, 3297–3305.

(86) Generalized Relativistic Effective Core Potentials (NRC "Kurchatov Institute" – PNPI). http://www.qchem.pnpi.spb.ru/recp (accessed on 20 July 2024).

(87) Boys, S.; Bernardi, F. The calculation of small molecular interactions by the differences of separate total energies. Some procedures with reduced errors. *Mol. Phys.* **1970**, *19*, 553–566.

(88) Sanville, E.; Kenny, S. D.; Smith, R.; Henkelman, G. Improved grid-based algorithm for Bader charge allocation. *J. Comput. Chem.* **2007**, *28*, 899–908.

(89) Tang, W.; Sanville, E.; Henkelman, G. A grid-based Bader analysis algorithm without lattice bias. *J. Phys.: Condens. Matter* **2009**, *21*, 084204.

(90) Demidov, Y. A.; Zaitsevskii, A.; Eichler, R. First principle based modeling of the adsorption of an element 120 atom on a gold surface. *Phys. Chem. Chem. Phys.* **2014**, *16*, 2268 – 2270.

(91) Santiago-Rodriguez, Y.; Herron, J. A.; Curet-Arana, M. C.; Mavrikakis, M. Atomic and molecular adsorption on Au (111). *Surf. Sci.* **2014**, *627*, 57–69.

(92) Grimme, S.; Ehrlich, S.; Goerigk, L. Effect of the damping function in dispersion corrected density functional theory. *J. Comput. Chem.* **2011**, *32*, 1456–1465.

(93) Caldeweyher, E.; Bannwarth, C.; Grimme, S. Extension of the D3 dispersion coefficient model. *J. Chem. Phys.* **2017**, *147*, 034112.

(94) Caldeweyher, E.; Ehlert, S.; Hansen, A.; Neugebauer, H.; Spicher, S.; Bannwarth, C.; Grimme, S. A generally applicable atomic-charge dependent London dispersion correction. *J. Chem. Phys.* **2019**, *150*, 154122.

(95) Friede, M.; Ehlert, S.; Grimme, S.; Mewes, J.-M. Do Optimally Tuned Range-Separated Hybrid Functionals Require a Reparametrization of the Dispersion Correction? It Depends. *J. Chem. Theory Comput.* **2023**, *19*, 8097–8107.

(96) Lide, D. R. *CRC Handbook of Chemistry and Physics, 85th Edition*; CRC Handbook of Chemistry and Physics, 85th Ed; Taylor & Francis, 2004.

(97) Saliba, N.; Parker, D.; Koel, B. E. Adsorption of oxygen on Au (111) by exposure to ozone. *Surf. Sci.* **1998**, *410*, 270–282.

(98) Baker, T. A.; Xu, B.; Liu, X.; Kaxiras, E.; Friend, C. M. Nature of oxidation of the Au (111) surface: Experimental and theoretical investigation. *J. Phys. Chem. C* **2009**, *113*, 16561–16564.

(99) Gligorovski, S.; Strekowski, R.; Barbati, S.; Vione, D. Environmental Implications of Hydroxyl Radicals (•OH). *Chem. Rev.* **2015**, *115*, 13051–13092.

(100) Ikeda, S.; Nakajima, T.; Hirao, K. A theoretical study of transition metal hydroxides: CuOH, AgOH and AuOH. *Mol. Phys.* **2003**, *101*, 105–110.

(101) Brooker, J.; Christensen, P.; Hamnett, A.; He, R.; Paliteiro, C. Combined scanning tunnelling microscopy and in situ Fourier transform infrared study of dioxygen reduction on gold. *Faraday Discuss.* **1992**, *94*, 339–360.

(102) Xu, B.; Liu, X.; Haubrich, J.; Madix, R. J.; Friend, C. M. Selectivity control in gold-mediated esterification of methanol. *Angew. Chem.* **2009**, *121*, 4270–4273.

(103) Xu, B.; Haubrich, J.; Baker, T. A.; Kaxiras, E.; Friend, C. M. Theoretical study of O-assisted selective coupling of methanol on Au (111). *J. Phys. Chem. C* **2011**, *115*, 3703–3708.

(104) Huzayyin, A.; Chang, J. H.; Lian, K.; Dawson, F. Interaction of Water Molecule with Au(111) and Au(110) Surfaces under the Influence of an External Electric Field. *J. Phys. Chem. C* **2014**, *118*, 3459–3470.

TOC Graphic

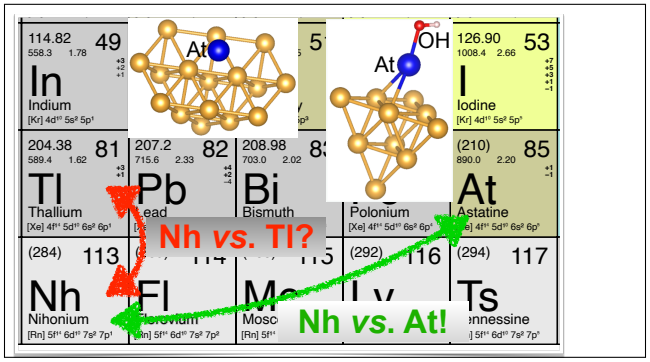

Table 6: Equilibrium distances R_e between the adatom and the surface layer of gold, adsorption energies E_{ads}, and vibrational frequencies ω_e for the adsorption complexes calculated with the 2c-RDFT/PBE0(-D4) method. Our E_{ads} values include ZPE contributions. Other theoretical and experimental data are also presented when available in the literature.

System	Method	R_e (Å)	$-E_{\text{ads}}$ (kJ/mol)	ω_e cm^{-1}
O–Au(111)	PBE0	1.28	244	427
	PBE0-D4	1.28	255	
	PBE0-D4-ZPE	1.28	247	
	Theory[91a]	1.30	211	382
	Experiment[97,98]	–	234 ± 33	380
OH–Au(111)	PBE0	1.70	118	317[b]
	PBE0-D4	1.70	131	
	PBE0-D4-ZPE	1.70	119	
	Theory[91a]	1.73	114	332
At–Au(111)	PBE0	2.57	137	122[b]
	PBE0-D4	2.57	164	
	PBE0-D4-ZPE	2.57	157	
	Theory[c 36]	2.57[d]	179	
	Theory[38]	2.56[d]	184	
	Theory[39]		189	
	Experiment[40]	–	147 ± 15	
AtOH–Au(111)	PBE0	2.61	98	114[b]
	PBE0-D4	2.61	126	
	PBE0-D4-ZPE	2.61	117	
	Theory[38]		185	
	Experiment[40]	–	100^{+20}_{-10}	–

[a] Relativistic effects and the Grimme dispersion correction (D3 or D4) are not taken into account.

[b] The O – Au(111) and At – Au(111) stretching modes make the leading ZPE contributions to binding energies.

[c] The At atom is in the hollow-3 adsorption position.

[d] For consistency, we convert the distances between At and the nearest Au atom (2.952 Å[36] and 2.94 Å[38]) to the distances between At and the plane of the closest layer of Au atoms.